Supporting Information

Conformationally Unambiguous Spin Label for Exploring the Binding Site Topology of Multivalent Systems

Sabrina Weickert[†], *Torben Seitz*[†], *William K. Myers*[⊥], *Christiane R. Timmel*[⊥], *Malte Drescher*[†]*, *Valentin Wittmann*[†]*

[†] Department of Chemistry and Konstanz Research School Chemical Biology (KoRS-CB), University of Konstanz, 78457 Konstanz, Germany

[⊥] Department of Chemistry and Centre for Advanced Electron Spin Resonance (CAESR), University of Oxford, South Parks Road, Oxford OX1 3QR, United Kingdom

Content

Chemical synthesis **S3**

Synthesis of MUeSLI^{GlcNAc} S4

Synthesis of MUeSLI^{Glc} S7

EPR experiments **S11**

Estimation of the binding affinity of MUeSLI^{GlcNAc} by cw EPR **S15**

Figures S2 – S12 ..... **S18**

Table S2 ..... **S30**

NMR Spectra **S31**

HPLC profiles of paramagnetic compounds **S34**

References **S35**

Chemical synthesis

General methods

Analytical thin layer chromatography (TLC) was carried out on silica gel 60 F_{254} coated aluminum sheets (Merck) with detection by UV light (λ = 254 nm). Additionally, following reagents were used for visualization of spots if applicable: iodine chamber, ethanolic ninhydrin solution (3 % w/v), anisaldehyde solution (135 mL EtOH, 5 mL H_2SO_4, 15 mL glacial acetic acid, 3.7 mL *p*-anisaldehyde), aqueous potassium permanganate (1 % w/v). After dipping into one of the described solutions, heating was applied. R_f-values were determined under chamber saturation. Preparative flash column chromatography (FC) was performed on silica gel Geduran 60 (40 -60 μm, Merck) with solvent systems specified. NMR spectra were recorded on an Avance III 400 from Bruker at rt. ^{1}H and ^{13}C NMR chemical shifts are referenced to the solvent signals ($CDCl_3$ δ_H = 7.26, δ_C = 77.1; [D_4]MeOH δ_H = 4.87, δ_C = 49.0). Signals were assigned with the help of two dimensional correlation spectroscopy (COSY, HSQC, TOCSY and HMBC). Semi-preparative RP-HPLC was conducted on a LC-20A prominence system from Shimadzu (pumps LC-20AT, auto sampler SIL-20A, column oven CTO-20AC, diode array detector SPD-M2OA, controller CBM-20A and software LC-solution). Used column: Eurospher 100 C18 (250 x 16 mm) from Knauer. A gradient of water with 0.1 % TFA (eluent A) and varying amounts of MeCN with 0.1 % TFA (eluent B) was used as mobile phase. Analytical LC-MS measurements were performed on an LCMS2020 instrument from Shimadzu (high pressure pumps LC-20 AD, autosampler SIL-20AT HAT, column oven CTO-20AC, UV-Vis detector SPD-20A, fluorescence detector RF-20A, controller CBM-20, ESI detector, software LC MS Solution). Used column: Nucleodur C_{18} Gravity, 3 μm (125 x 4 mm) from Macherey Nagel. A gradient of water with 0.1 % formic acid (eluent A) and varying amounts of MeCN with 0.1 % formic acid (eluent B) was used as mobile phase (flow: 0.4 mL min^{-1}). Mass spectra with electrospray ionization (ESI-MS) were recorded on an Esquire 3000 plus instrument from Bruker with electron spray ionization or at the LC-MS instrument LCMS2020 from Shimadzu as specified above. Samples were prepared in MeOH (approx. 1 μg min^{-1}).

Synthesis of MUeSLI^{GlcNAc}

(4-(2-Acetamido-3,4,6-tri-*O*-acetyl-2-deoxy-β-D-glucopyranosyl)phenyl)boronic acid pinacol ester (2)

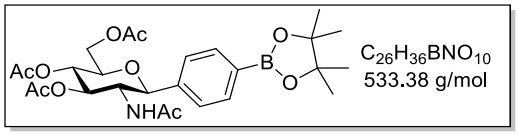

1-(2-Acetamido-3,4,6-tri-*O*-acetyl-2-deoxy-*β*-D-glucopyranosyl)-4-bromobenzene **1**[1] (317 mg, 0.651 mmol), bis(pinacolato)diboron (199 mg, 0.782 mmol), $PdCl_2$(dppf) (18 mg, 0.022 mmol), dppf (36 mg, 0.065 mmol), and KOAc (192 mg, 1.95 mmol) were placed in a Schlenk flask and heated under vacuum to 80 °C for 5 h. Degassed DMF (8 mL) was added and the reaction mixture was stirred overnight at 80 °C. The solvent was removed under reduced pressure and the residue was dissolved in EtOAc and washed with brine. After drying over $MgSO_4$, the solvent was evaporated and the residue purified by FC (petroleum ether/EtOAc 1:3) to yield boronic acid pinacol ester **2** (231 mg, 66 %) as white amorphous solid. $\boldsymbol{R_f}$ = 0.42 (petroleum ether/EtOAc 1:3), $KMnO_4$; ^{1}**H NMR (400 MHz, $CDCl_3$)**: δ [ppm] = 7.74 (d, *J* = 7.8 Hz, 2 H, Ar-H), 7.32 (d, *J* = 7.8 Hz, 2 H, Ar-H), 5.96 (d, *J* = 9.4 Hz, 1 H, NH), 5.31 (t, *J* = 9.6 Hz, 1 H, H-3), 5.21 (t, *J* = 9.6 Hz, 1 H, H-4), 4.45 (d, *J* = 10.1 Hz, 1 H, H-1), 4.26 (dd, *J* = 12.2 Hz, 4.8 Hz, 1 H, H-6a), 4.20-4.10 (m, 2 H, H-6b, H-2), 3.84-3.80 (m, 1 H, H-5), 2.04 (s, 3 H, CH_3), 2.02 (s, 3 H, CH_3), 2.00 (s, 3 H, CH_3), 1.65 (s, 3 H, CH_3), 1.29 (s, 12 H, CH_3); **^{13}C NMR (100 MHz, $CDCl_3$):** δ [ppm] =171.2, 170.9, 169.8, 169.5 (C=O), 140.0, 134.8, 126.7 (C^{Ar}), 83.9 ($\underline{C}(CH_3)_2$), 81.0 (C-1), 76.2 (C-5), 74.4 (C-3), 69.0 (C-4), 62.7 (C-6), 55.1 (C-2), 25.0, 24.9, 24.9, 23.0 (CH_3), 20.8 ($C(\underline{C}H_3)_2$); **LC-MS**: t_r = 3.26 min (80-100 % B in 10 min); **ESI-MS**: *m/z* calcd for $C_{26}H_{36}BNO_{10}$ + H^+: 534.2 $[M+H]^+$, found: 534.2.

(4-(2-Acetamido-3,4,6-tri-*O*-acetyl-2-deoxy-*β*-D-glucopyranosyl)phenyl)boronic acid (3)

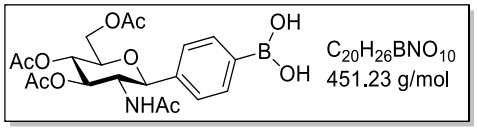

Pinacol ester **2** (230 mg, 0.431 mmol) was dissolved in acetone/H_2O 1:1 (20 mL), NH_4OAc (53 mg, 0.69 mmol) and $NaIO_4$ (148 mg, 0.69 mmol) were added, and the suspension was stirred at rt

for 2 d. The acetone was removed under reduced pressure and the aqueous remainder was extracted three times with EtOAc. The combined organic layers were washed with brine, dried over $MgSO_4$, and concentrated under reduced pressure to give boronic acid **3** (162 mg, 83 %) as a white amorphous solid. $\boldsymbol{R_f}$ = 0.10 (petroleum ether/EtOAc 1:3), $KMnO_4$; **^{1}H NMR (400 MHz, $CDCl_3$)**: δ [ppm] = 8.01 (s, 2 H, $B(OH)_2$), 7.90 (d, *J* = 9.5 Hz, 1 H, NH), 7.71 (d, *J* = 7.9 Hz, 2 H, Ar-H), 7.28 (d, *J* = 7.9 Hz, 2 H, Ar-H), 5.18 (t, *J* = 9.8 Hz, 1 H, H-3), 5.01 (t, *J* = 9.8 Hz, 1 H, H-4), 4.52 (d, *J* = 10.3 Hz, 1 H, H-1), 4.16 (dd, *J* = 12.4 Hz, 5.2 Hz, 1 H, H-6a), 4.07 (dd, *J* = 12.4 Hz, 2.4 Hz, 1 H, H-6b), 4.03-3.92 (m, 2 H, H-2, H-5), 2.01 (s, 6 H, 2 x CH_3), 1.91 (s, 3 H, CH_3), 1.54 (s, 3 H, CH_3); **^{13}C NMR (100 MHz, $CDCl_3$)**: δ [ppm] =170.1, 169.8, 169.4, 168.6 (C=O), 139.6, 133.7, 126.3 (C^{Ar}), 79.4 (C-1), 75.0 (C-5), 74.2 (C-3), 68.9 (C-4), 62.4 (C-6), 53.9 (C-2), 22.4, 20.6, 20.5, 20.4 (CH_3); **LC-MS**: t_r = 3.85 min (80-100 % B in 10 min); **ESI-MS**: *m/z* calcd for $C_{20}H_{26}BNO_{10}$ + H^+: 452.1 $[M+H]^+$, found: 452.0.

1-(4-(2-Acetamido-3,4,6-tri-*O*-acetyl-2-deoxy-β-D-glucopyranosyl)phenyl)-3,3,5,5-tetramethylpiperazine-2,6-dione (5)

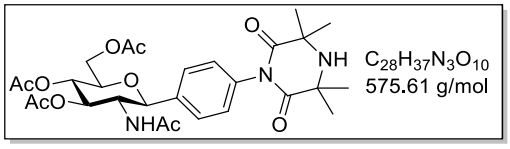

A mixture of boronic acid **3** (80 mg, 0.177 mmol), 3,3,5,5-tetramethylpiperazine-2,6-dione **4**[2-3] (30 mg, 0.177 mmol), $Cu(OAc)_2$ (32 mg, 0.177 mmol), and dry Et_3N (35 µL, 0,248 mmol) in dry DMSO (4 mL) was stirred with molecular sieves (4 Å) at rt under an oxygen atmosphere for 7 d. The suspension was filtered through Celite, diluted with water, and extracted thrice with EtOAc. The combined organic layers were dried over $MgSO_4$ and concentrated under reduced pressure. Half of the crude product **5** was directly used in the next step. For analysis, a small amount was purified by FC (EtOAc with 1 % NEt_3). $\boldsymbol{R_f}$ = 0.15 (EtOAc/NEt_3 100:1), anisaldehyde; **^{1}H NMR (400 MHz, $CDCl_3$)**: δ [ppm] = 7.43 (d, *J* = 8.4 Hz, 2 H, Ar-H), 7.05 (d, *J* = 8.4 Hz, 2 H, Ar-H), 5.48-5.41 (m, 2 H, H-3, NH), 5.19 (t, *J* = 9.8 Hz, 1 H, H-4), 4.67 (d, *J* = 10.2 Hz, 1 H, H-1), 4.25 (dd, *J* = 12.4 Hz, 5.2 Hz, 1 H, H-6a), 4.12 (dd, *J* = 12.4 Hz, 2.2 Hz, 1 H, H-6b), 4.09-4.02 (m, 1 H, H-2), 3.87-3.83 (m, 1 H, H-5), 2.07 (s, 3 H, $C(O)CH_3$), 2.05 (s, 3 H, $C(O)CH_3$), 2.03 (s, 3 H, $C(O)CH_3$), 1.74 (s, 3 H, $C(O)CH_3$), 1.52 (s, 12 H, $C(CH_3)_2$); **^{13}C NMR (100 MHz, $CDCl_3$)**:

δ[ppm] =171.1, 171.0, 170.1, 169.7 (C=O), 128.6-128.5 (C^{Ar}), 80.1 (C-1), 76.4 (C-5), 73.9 (C-3), 69.1 (C-4), 62.8 (C-6), 55.8 (C-2), 28.5 ($C(\underline{C}H_3)_2$), 23.3, 20.9, 20.9, 20.8 ($C(O)\underline{C}H_3$); **LC-MS**: t_r = 9.50 min (20-95 % B in 20 min); **ESI-MS**: *m/z* calcd for $C_{28}H_{37}N_3O_{10}$ + H^+: 576.6 $[M+H]^+$, found: 576.3.

1-(4-(2-Acetamido-3,4,6-tri-*O*-acetyl-2-deoxy-β-D-glucopyranosyl)phenyl)-3,3,5,5-tetramethyl-4-oxylpiperazine-2,6-dione (6)

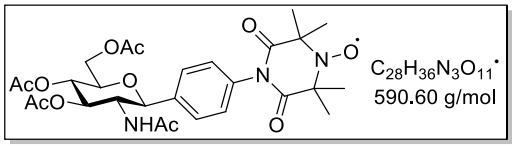

To an ice-cold solution of crude product **5** (half of the amount obtained in the preceding experiment, max. 88 μmol) in dry CH_2Cl_2 (5 mL), mCPBA (28 mg, 164 μmol) was added. The solution was stirred for 15 min at 0 °C and for 5 h at rt. The solvent was removed under reduced pressure and the residue was purified by FC (petroleum ether/EtOAc 1:4) to give nitroxide **6** (39 mg, 75 % from **3**) as a white amorphous solid. $\boldsymbol{R_f}$ = 0.32 (petroleum ether/EtOAc 1:4), anisaldehyde; **LC-MS**: t_r = 12.18 min (20-95 % B in 20 min); **ESI-MS**: *m/z* calcd for $C_{28}H_{36}N_3O_{11}$ + H^+: 591.2 $[M+H]^+$, found: 591.3.

1-(4-(2-Acetamido-2-deoxy-β-D-glucopyranosyl)phenyl)-3,3,5,5-tetramethyl-4-oxylpiperazine-2,6-dione (MUeSLI^{GlcNAc})

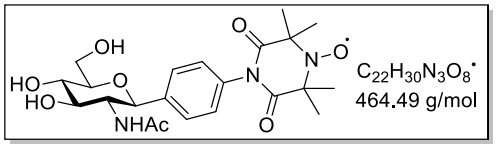

Nitroxide **6** (9 mg, 15 μmol) was dissolved in a solution of NaOMe in dry MeOH (35 mM, 2 mL) and stirred at rt. After completion of the reaction, the mixture was neutralized with ion-exchange resin Amberlite IR-120 (H^+ form), filtered, and the solvent was removed under reduced pressure. Lyophilization gave MUeSLI^{GlcNAc} (7 mg, quant.) as a white amorphous solid. $\boldsymbol{R_f}$ = 0.18 (CH_2Cl_2/MeOH 10:1), anisaldehyde; **LC-MS**: t_r = 2.41 min (20-95 % B in 20 min); **ESI-MS**: *m/z* calcd for $C_{22}H_{30}N_3O_8$ + MeOH+ H^+: 497.2 $[M+MeOH+H]^+$, found: 497.2.

Synthesis of MUeSLI^{Glc}

The synthesis of MUeSLI^{Glc} started from known 3,4,6-tetra-*O*-benzyl-D-glucopyranolactone **7**[4] as depicted in Scheme S1.

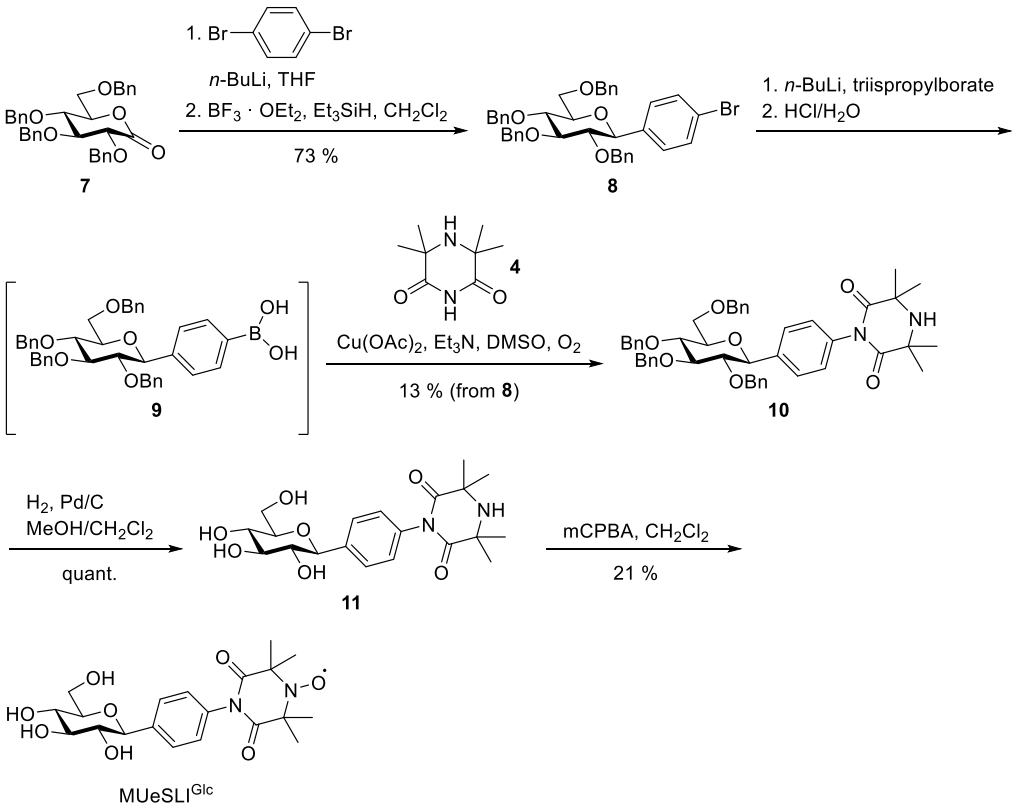

Scheme S1. Synthesis of MUeSLI^{Glc}.

1-(2,3,4,6-tetra-*O*-Benzyl-β-D-glucopyranosyl)-4-bromobenzene (8)

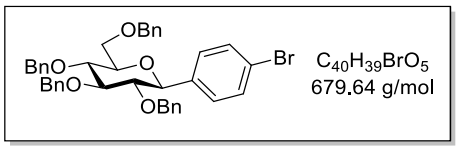

1,4-Dibromobenzene (1.07 mL, 8.34 mmol) was dissolved in dry THF (42 mL) and cooled to –78 °C. *n*-BuLi (2.5 M in hexane, 3.34 mL, 8.34 mmol) was added slowly keeping the internal temperature not higher than –65 °C. The mixture was stirred at –78 °C for 30 min and 3,4,6-tetra-*O*-benzyl-D-glucopyranolactone **7**[4] (3.0 g, 5.56 mmol), dissolved in dry THF (16.5 mL), was added slowly. The reaction mixture was stirred for 1 h at –78 °C, warmed up to –30 °C, and

quenched with water. The mixture was extracted with Et_2O and dried over $MgSO_4$. After removal of the solvent under reduced pressure, the remaining oil was dissolved in dry CH_2Cl_2 (28 mL) and cooled to –78 °C. Et_3SiH (1.78 mL, 11.12 mmol) and $BF_3 \cdot Et_2O$ (1.37 mL, 11.12 mmol) were added and the reaction mixture was warmed up to rt overnight. Sat aq $NaHCO_3$ solution was added and the mixture extracted with CH_2Cl_2 (3 x) and dried ($MgSO_4$). After removal of the solvent under reduced pressure, the product was crystallized from a minimum amount of petroleum ether yielding *C*-glycosyl compound **8** (2.76 g, 73 %) as a white amorphous solid. $\boldsymbol{R_f}$ = 0.28 (petroleum ether/EtOAc 7:1); **^{1}H NMR (400 MHz, $CDCl_3$)**: δ [ppm] = 7.53-7.19 (m, 22 H, Ar-H), 6.99-6.92 (m, 2 H, Ar-H), 4.99-4.85 (m, 3 H, CH_2), 4.70-4.62 (m, 2 H, CH_2), 4.61-4.55 (m, 1 H, CH_2), 4.46 (d, J = 10.5 Hz, 1H, CH_2), 4.21 (d, J = 9.3 Hz, 1 H, H-1), 3.89 (d, J = 10.5 Hz, 1 H, CH_2), 3.83-3.74 (m, 4 H, H-3, H-4, H-6ab), 3.63-3.58 (m, 1 H, H-5), 3.48-3.42 (m, 1 H, H-2); **^{13}C NMR (100 MHz, $CDCl_3$)** δ = 138.7-127.7 (C^{Ar}), 86.9 (C-4), 84.1 (C-2), 81.0 (C-1), 79.5 (H-5), 78.4 (C-3), 75.8 (C^{Bn}), 75.3 (C^{Bn}), 75.1 (C^{Bn}), 73.6 (C^{Bn}), 69.2 (C-6); **LC-MS**: t_r = 10.50 min (90-100 % B in 10 min); **ESI-MS**: *m/z* calcd for $C_{40}H_{39}BrO_5 + Na^+$: 703.2 $[M+Na]^+$, found: 702.8.

1-(4-(2,3,4,6-tetra-*O*-Benzyl-β-d-glucopyranosyl)phenyl)-3,3,5,5-tetramethylpiperazine-2,6-dione 10

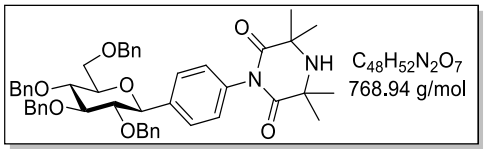

To a solution of *C*-glycosyl compound **8** (200 mg, 0.29 mmol) in THF (8 mL), *n*-BuLi (2.5 M in hexane, 0.68 mL, 1.74 mmol) and triisopropylborate (1.6 mL, 7.06 mmol) were added under a N_2 atmosphere at –78 °C. The reaction mixture was stirred for 10 min at –78 °C and for 1 h at rt. The reaction mixture was cooled to 0 °C and sat aq NH_4Cl solution was added. After the addition of EtOAc, the solution was slightly acidified with 1 M HCl and extracted with EtOAc (3 x). The combined organic layers were washed with brine, dried ($MgSO_4$) and concentrated. The obtained crude (4-(2,3,4,6-tetra-*O*-benzyl-β-D-glucopyranosyl)phenyl)boronic acid **9** (187 mg) was mixed with 3,3,5,5-tetramethylpiperazine-2,6-dione **4** (49 mg, 0.29 mmol), $Cu(OAc)_2$ (53 mg, 0.29 mmol), dry Et_3N (57 μL, 0.41 mmol), and molecular sieves (4 Å) in dry DMSO (6 mL) and stirred under an oxygen atmosphere for 7 d at rt. The suspension was filtered through Celite, diluted with

water, and extracted thrice with EtOAc. The combined organic layers were washed with brine, dried over $MgSO_4$ and concentrated under reduced pressure. Purification by semi-preparative HPLC (80-100% B in 20 min) yielded **10** (29 mg, 13 % from **8**) as a white amorphous solid. $\boldsymbol{R_f}$ = 0.14 (petroleum ether/EtOAc 2:1), anisaldehyde; **^{1}H NMR (400 MHz, $CDCl_3$)**: δ [ppm] = 7.46 (d, J = 8.0 Hz, 2 H, Ar-H), 7.40-7.12 (m, 18 H, Ar-H), 7.01 (d, J = 8.0 Hz, 2 H, Ar-H), 6.90-6.88 (m, 2 H, Ar-H), 4.92-4.78 (m, 3 H, CH_2), 4.59-4.48 (m, 3 H, CH_2), 4.37 (d, J = 10.0 Hz, 1 H, CH_2), 4.21 (d, J = 9.4 Hz, 1 H, H-1), 3.78-3.67 (m, 5 H, H-3, H-4, H-6, CH_2), 3.55-3.51 (m, 1 H, H-2), 3.44-3.40 (m, 1 H, H-5), 1.46 (s, 12 H, CH_3); **^{13}C NMR (100 MHz, $CDCl_3$):** δ [ppm] = 176.7 (C=O), 139.7, 138.8, 138.4, 138.3, 137.6, 135.6, 128.9-127.6 (C^{Ar}), 86.9 (C-3), 84.5 (C-5), 81.3 (C-1), 79.6 (C-2), 78.5 (C-4), 75.9, 75.4, 75.3, 73.7 (C^{Bn}), 69.3 (C-6), 56.2 ($\underline{C}(CH_3)_2$), 28.7 (CH_3), **LC-MS**: t_r = 7.7 min (80-100 % B in 10 min); **ESI-MS**: *m/z* calcd for $C_{48}H_{52}N_2O_7$ + Na: 791.4 $[M+Na]^+$, found: 791.5.

1-(4-(β-D-Glucopyranosyl)phenyl)-3,3,5,5-tetramethylpiperazine-2,6-dione (11)

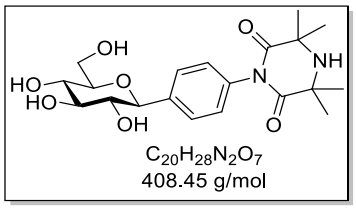

Perbenzylated *C*-glycosyl compound **10** (25 mg, 0.032 mmol) was dissolved in MeOH (0.6 mL) and hydrogenation catalyst (10 % palladium on activated charcoal, 10 mg) was added. The reaction was stirred under an H_2 atmosphere at rt for 3 h. The mixture was filtered through Celite, MeOH was removed under reduced pressure, and the remainder was lyophilized to give debenzylated **11** (13 mg, quant) as a white amorphous solid. $\boldsymbol{R_f}$ = 0.1 (CH_2Cl_2/MeOH 7:1), anisaldehyde; **^{1}H NMR (400 MHz, [D$_4$]MeOD)**: δ [ppm] = 7.58 (d, J = 8.0 Hz, 2 H, Ar-H), 7.14 (d, J = 8.0 Hz, 2 H, Ar-H), 4.24 (d, J = 9.4 Hz, 1 H, H-1), 3.91-3.88 (m, 1 H, H-6a), 3.75-3.70 (m, 1 H, H-6b), 3.53-3.40 (m, 3 H, H-3, H-4, H-5), 3.36 (t, J = 9.0 Hz, 1 H, H-2), 1.60 (s, 12 H, CH_3); **^{13}C NMR (100 MHz, [D$_4$]MeOD):** δ [ppm] = 178.1 (C=O), 141.5, 136.4, 129.7, 129.2 (C^{Ar}), 83.1 (C-1), 82.2 (C-5), 79.6 (C-3), 71.9 (C-2), 71.9 (C-4), 61.1 (C-6), 57.8 ($\underline{C}(CH_3)_2$, 27.9.(CH_3); **LC-MS:** t_r = 2.20 min (40-80 % B in 5 min); **ESI-MS**: *m/z* calcd for $C_{20}H_{28}N_2O_7$ + MeCN + H^+: 450.2 $[M+MeCN+H]^+$, found: 450.2.

1-(4-(β-D-Glucopyranosyl)phenyl)-3,3,5,5-tetramethyl-4-oxylpiperazine-2,6-dione (MUeSLI^{Glc})

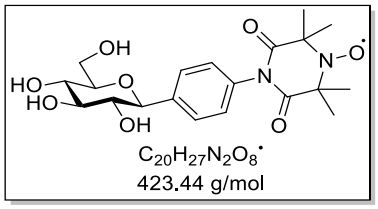

To an ice-cold solution of amine **11** (10 mg, 25 μmol) in dry CH_2Cl_2 (1 mL), mCPBA (8.6 mg, 50 μmol) was added. The solution was stirred for 15 min at 0 °C and for 5 h at rt. The solvent was removed under reduced pressure and the residue was purified by FC (CH_2Cl_2/MeOH 10:1) yielding MUeSLI^{Glc} (2.2 mg, 21 %) as a white amorphous solid. R_f = 0.18 (CH_2Cl_2/MeOH 10:1), anisaldehyde; **LC-MS**: t_r = 3.45 min (40-80 % B in 5 min); **ESI-MS**: *m/z* calcd for $C_{20}H_{27}N_2O_8$ + H_2O+ H^+: 442.2 $[M+H_2O+H]^+$, found: 442.2.

EPR experiments

Sample preparation

Lectin solutions were prepared from WGA as purchased from Sigma as lyophilized powder and with no carbohydrate bound. The lectin was dissolved in MilliQ water at neutral pH and concentrations in the sample solutions were determined spectrophotometrically with a molar extinction coefficient $E_{280\ nm}$ = 59201 $Lmol^{-1}cm^{-1}$ and a molecular weight of 36 kDa per WGA dimer.

Ligand solutions of MUeSLI were prepared by dissolving the lyophilized ligand in MilliQ water. The spin label concentration was determined by EPR spectroscopy using the reference free spin counting function of the EMXnano (Bruker Biospin).

For EPR measurements performed with $MUeSLI^{GlcNAc}$ in the presence of WGA, the ligand and lectin solutions were mixed in the desired ratio, lyophilized and stored at -80 °C. For EPR experiments the samples were resuspended in MilliQ water or D_2O for cw EPR or DEER experiments, respectively. For measurements at cryogenic temperatures 20 % (v/v) glycerol (or [D_8]glycerol for DEER experiments) were added to the samples as cryoprotectant.

X-band EPR spectroscopy

$MUeSLI^{GlcNAc}$ was characterized by cw EPR at X-band frequency in aqueous solution of 50 μM concentration. Cw X-band EPR (9.398 GHz) experiments were performed on an ELEXSYS E580 spectrometer equipped with a SuperHighQ resonator (both Bruker Biospin) and a helium flow cryostat ESR900 (Oxford Instruments) for temperature control. Measurement parameters were adjusted such that the spectral line shape was not distorted by overmodulation or saturation effects. Samples for cryogenic measurements were loaded into quartz tubes with 3 mm inner diameter (I.D.) and measured after shock freezing in liquid nitrogen. Cryogenic measurements were performed at T = 120 K. A full spectral simulation of the powder spectrum was performed using the ‘pepper’ function of the EasySpin toolbox and homewritten Matlab scripts.[5] Samples for room temperature measurements were loaded into glass capillaries with 1 mm I.D.. Discussion of the spectra is shown in Figure S1.

W-band EPR spectroscopy

For measurements of pure MUeSLI^{GlcNAc}, sample solutions of 200 μM concentration were prepared. Samples were filled into quartz capillaries with 0.7 mm I.D. and shock frozen in liquid nitrogen before measurement.

Cw EPR experiments in W-band (93.983 GHz) were performed at T = 175 K. W-band EPR spectra were recorded on an ELEXSYS E680 spectrometer equipped with a 61 mm bore AG BZH 02/6T/54-S77A superconducting magnet and an EN600-1021H Teraflex W-band pulsed ENDOR resonator (all Bruker Biospin). Temperature was maintained with an ITC-509 temperature controller and a CF-935SW helium flow cryostat (both Oxford Instruments). Measurement parameters were adjusted such that the spectral line shape was not distorted by overmodulation or saturation effects.

As a field standard a solution of DPPH in benzene was used and the corresponding g-value was taken from the literature.[6-7] The DPPH solution was enclosed in 0.15 mm I.D. (0.25 mm O.D.) quartz glass capillaries and introduced into the W-band sample capillaries together with the MUeSLI^{GlcNAc} solution. In order to confirm uniformity of the magnetic field over the sweep range also a manganese standard in MgO was measured at the same conditions. All recorded absorption EPR signals were screened for dispersion, but the apparent phase deviation was found to be negligible. Noisy spectra were smoothed by a moving average filter while making sure that no spectral features were lost and the number of points per spectral feature was still sufficient after smoothing. g-tensor principal components were determined by full spectral simulation using the function ‘pepper’ from the EasySpin toolbox.[5]

Q-band DEER

DEER experiments with WGA and MUeSLI^{GlcNAc} were performed at MUeSLI^{GlcNAc} concentrations of 400 μM in the presence of 20 % (v/v) glycerol-d_8. MUeSLI^{GlcNAc} was added to WGA in 2-fold and 16-fold molar excess, corresponding to WGA concentrations of 200 and 25 μM, respectively. Samples were loaded into quartz sample tubes with 1 mm I.D. and shock frozen in liquid nitrogen before measurement.

The experiments were performed using an ELEXSYS E580 spectrometer equipped with an EN5107D2 Q-band EPR probe head (both Bruker Biospin) and a 10 W solid state amplifier. A CF935 helium gas flow system (Oxford Instruments) was used for temperature control. Experiments were performed at T = 50 K. The DEER experiment was performed using a dead-time free four-pulse sequence.[8] The echo amplitude was recorded as a function of the dipolar evolutions time t. The corresponding EPR spectrum was obtained by field-swept echo acquisition and the pump and observer pulses were positioned on the global maximum and close to the most intense local maximum (shifted by 50 MHz) of the spectrum, respectively. The pump pulse length was adjusted in order to obtain a flip angle of π resulting in a pulse length of 22 and 26 ns for samples containing 25 and 200 μM WGA, respectively. The observer pulse sequence was adjusted to reach flip angles $\frac{\pi}{2}$ and π resulting in corresponding pulse lengths of 26 or 22 and 52 or 44 ns for $\frac{\pi}{2}$ and π pulses, respectively, for samples containing 25 and 200 μM WGA, respectively. The pulse separation time τ_1 was 400 ns and the dipolar evolution time τ_2 was 7000 ns. Nuclear modulation artifacts of deuterated buffer were suppressed by variation of interpulse delay τ_1 by averaging 8 traces with $\Delta\tau_1$ = 16 ns. An eight-step phase cycle was used. A complete DEER experiment was performed as a 2D experiment, where one dimension was the time axis and the second dimension was the axis of individual scans. 20 and 35 individual scans were recorded for samples containing 200 and 25 μM WGA, respectively. The scans were subjected to phase correction individually and subsequently summarized.

DEER data sets were analyzed using the DeerAnalysis 2016 software package for MATLAB.[9] Extraction of the dipolar evolution function was achieved by background correction with a 3-dimensional homogeneous background function. Background-corrected data were analyzed by model-free Tikhonov regularization. The optimum regularization parameter α (Figure S5) was determined using the L-curve criterion. The resulting distance distributions were validated by the validation tool of the DeerAnalysis 2016 software by varying the background start (20 different values) and noise level (5 different values) during the regularization procedure. All resulting distance distributions are depicted as grey shaded areas in the distance distributions shown in Figure S4. Figure 3 in the main text shows the distance distributions *P(r)* normalized such that $\int P(r) = 1$.

For analysis of the reliability of the distance distributions, the 2D DEER data were split in half by summarizing either the even or the odd scans of the DEER experiment individually. The resulting data sets were subsequently analyzed independently as described above (Figure S6).

The phase memory time T_m of a DEER sample was measured with a Hahn echo experiment. The echo intensity was determined at varying interpulse delays and the resulting exponential decay was fitted as described in Figure S6.

Estimation of the binding affinity of MUeSLI^{GlcNAc} by cw EPR

For the determination of the binding site topology with MUeSLI, the binding affinity of the MUeSLI ligand needs to be strong enough to make a distance determination with DEER possible, yet the affinity should be weak enough in order to avoid multi-spin contributions to the distance distribution.

For non-modified monovalent GlcNAc as a ligand for WGA dissociation constants K_d between 2 and 2.5 mM have been reported.[10-11] Upon attachment of a rigid spin label side chain to GlcNAc, the binding affinity is expected to decrease for the resulting MUeSLI^{GlcNAc}. A classical method for determination of the dissociation constant K_d is isothermal titration calorimetry (ITC). However, ITC would require a very high amount of ligand material at such low binding affinities, and we thus refrained from determination of the exact dissociation constant K_d. However, the precise determination of the binding affinity is not of key importance to our study.

In order to roughly estimate the binding affinity, cw EPR spectra of 50 μM MUeSLI^{GlcNAc} in the absence and in the presence of 4-fold (200 μM) and 8-fold (400 μM) molar excess of WGA were recorded.

The dissociation constant for the interaction of a ligand L with a binding site B of a protein is defined as

$$K_d = \frac{c(L)c(B)}{c(LB)}$$

where c(L), c(B) and c(LB) are the equilibrium concentrations of ligand L, binding sites B and ligand-binding site complex after the reaction is completed, respectively.

For the association of GlcNAc or MUeSLI^{GlcNAc} with a binding site of WGA we assume, that the binding of several monovalent ligands to arbitrary binding sites of WGA occurs completely independent from each other without any effects of cooperativity in accordance with earlier results for monomeric GlcNAc ligands.[10]

Figure S1 displays the cw EPR spectra. When normalized to maximum intensity (not shown), the resulting spectral shapes in the absence and presence of WGA deviate only slightly. This suggests a low binding affinity of MUeSLI^{GlcNAc} towards WGA as expected. The spectral changes are too

small to perform a reliable analysis with two-component spectral simulations in order to determine the fractions of bound and unbound ligand and thus the binding affinity.

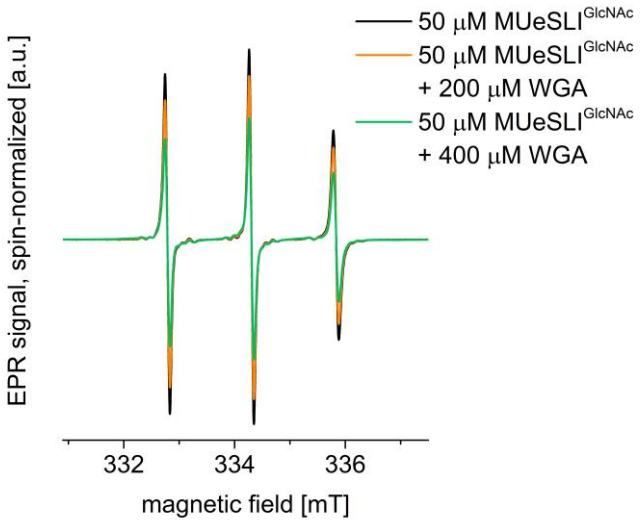

Figure S1: cw EPR spectra of MUeSLI^{GlcNAc} in the absence and presence of WGA normalized to the number of spins. cw EPR spectra of 50 μM MUeSLI^{GlcNAc} recorded in the absence (black) and presence of 200 μM (orange) and 400 μM (green) WGA, respectively, normalized to the number of spins. The decrease in peak heights upon adding more WGA indicates, that the spectral intensity is distributed in a broader spectral range, which is in agreement with MUeSLI^{GlcNAc} immobilized by binding to WGA.

However, upon normalization of the cw EPR spectra to the numbers of spins (Figure S1), the spectral changes upon addition of WGA become more obvious. The immobilization of the spin-labeled MUeSLI^{GlcNAc} upon binding to WGA manifests in an outwards shift of spectral intensity from the peak positions, thereby leading to a reduction of the absolute height of the spectra recorded in the presence of WGA. In order to roughly estimate a dissociation constant K_d from the spectra, we assume, that the peak height of the central peak indicates the amount of free ligand, while the reduction of central peak intensity is attributed to the fraction of bound ligand, which is immobilized and thus converts to spectral intensity shifted away from the peak. Thus, the central peak height of 50 μM MUeSLI^{GlcNAc} corresponds to 100 % free ligand, while the loss in central peak intensity for the spectra recorded in the presence of WGA deliver the fractions of bound ligand. Table S1 shows the peak heights and corresponding fractions of bound and unbound ligand, as well as the estimated dissociation constants K_d for 4-fold and 8-fold molar excess of WGA, respectively.

Of course, the result of this analysis represents only a very rough estimate of the dissociation

constant, as is obvious from the huge differences in K_d obtained for 4-fold and 8-fold excess of WGA, respectively. Apart from typical inaccuracies of spin normalization, the assumption that all spectral intensity at the peak positions vanishes in case of spin label immobilization is certainly imprecise. However, with all due caution one can conclude that the conformationally unambiguous spin label side chain attached to GlcNAc reduces the affinity of MUeSLI^{GlcNAc} towards WGA to approximately $K_d \approx 5$ mM.

Table S1: K_d values estimated from cw EPR spectra.

	central peak intensity [a.u.]	**c(free ligand)**	**c(bound ligand)**	**K_d**
50 μM MUeSLI^{GlcNAc}	5.63	50 μM	-	-
4-fold WGA	4.86	43 μM	7 μM	7.5 mM
8-fold WGA	3.62	32 μM	18 μM	4.3 mM

Figures S2 – S12

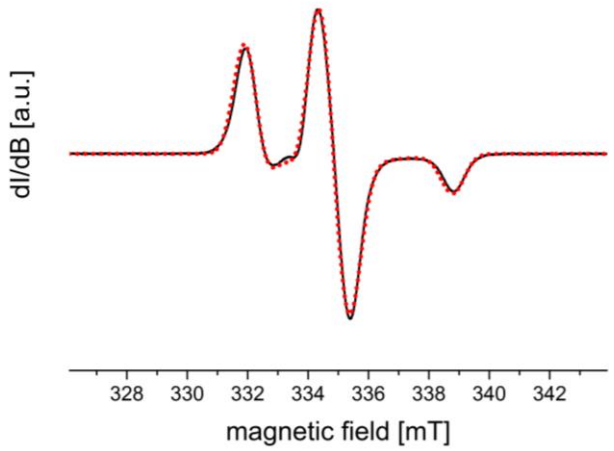

Figure S2: cw-EPR spectra of MUeSLI^{GlcNAc} recorded at X-band frequency. Cw X-band EPR spectrum of 50 μM MUeSLI^{GlcNAc} recorded in frozen glassy solution at T = 120 K containing 20 % (v/v) glycerol. Experimental data are shown in black, a full spectral simulation is shown in red (parameters see Table ST1).

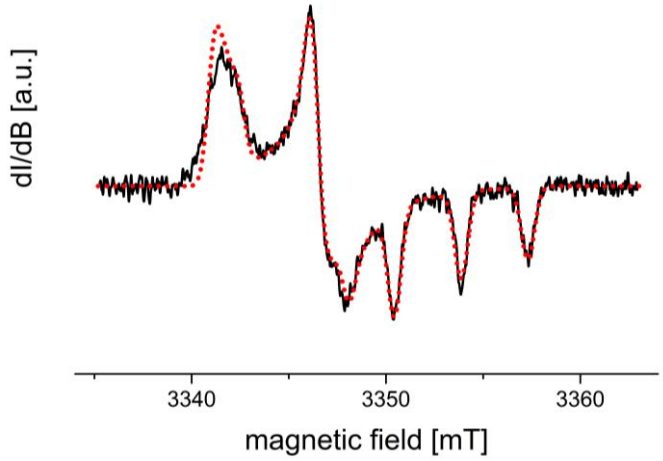

Figure S3: cw-EPR spectrum of MUeSLI^{GlcNAc} recorded at W-band frequency. Cw EPR spectrum of MUeSLI^{GlcNAc} recorded at W-band frequency at T = 175 K in frozen glassy solution (black). A full spectral simulation (red) is in good agreement with the experimental data. The corresponding parameters are given in Table ST1.

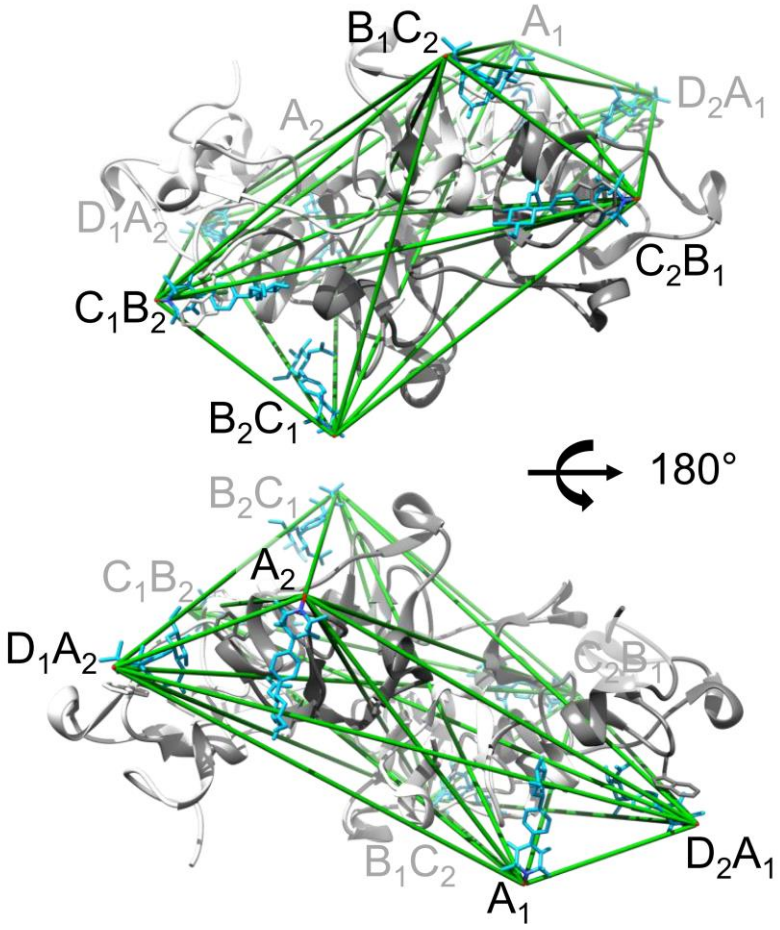

Figure S4: Protein structure analysis. An overlay of the MUeSLI^{GlcNAc} structure (cyan) and the protein structural model 2X52[12] (dark and light gray for different protomers) was performed using the UCSF Chimera software package. Distances between the O-atoms of the nitroxide radicals of MUeSLI^{GlcNAc} positioned in the eight GlcNAc binding sites of WGA were determined using the distance measurement tool of the UCSF Chimera software (green bars). Binding sites are labeled black and gray, depending whether they are on the facing or the far side of the protein graphics, respectively. All protein graphic images were produced using the UCSF Chimera package from the Computer Graphics Laboratory, University of California, San Francisco (supported by NIH P41 RR-01081).[13]

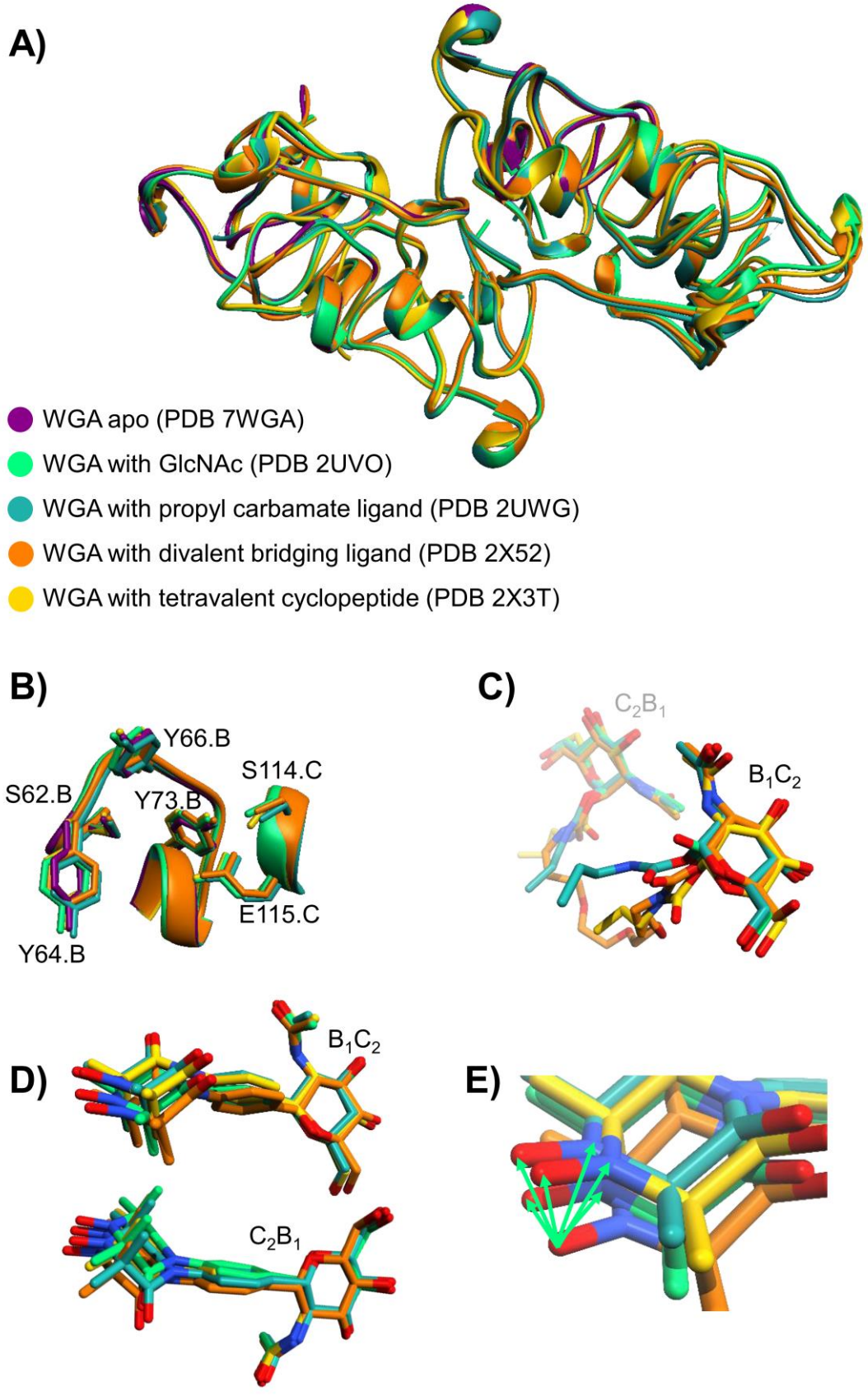
A)
WGA apo (PDB 7WGA)
WGA with GlcNAc (PDB 2UVO)
WGA with propyl carbamate ligand (PDB 2UWG)
WGA with divalent bridging ligand (PDB 2X52)
WGA with tetravalent cyclopeptide (PDB 2X3T)
B)
Y66.B
S114.C
S62.B
Y73.B
E115.C
Y64.B
C)
C2B1
B1C2
D)
B1C2
C2B1
E)

Figure S5: Protein dynamics. This figure shows a superposition of several crystal structural models obtained for WGA in its apo state (PDB 7WGA[14]) and co-crystallized with various ligands, differing in valency as well as scaffold architecture (PDB 2UVO, 2UWG, 2X52 and 2X3T[12]). The superposition was performed using the UCSF Chimera software package.[13] A) shows the general protein architecture. Upon binding of the ligands no large-scale conformational transitions occur. B) Exemplarily, the residues relevant for ligand-binding in binding site B_1C_2 are depicted in the presence and absence of ligands. Capital letters behind the residue number indicate the protein domain the respective residues belong to. Side chain reorientations are small upon ligand binding. C) shows the superposition of the various ligands present in the crystal structures in binding sites B_1C_2 and C_2B_1 in the background (amino acids not shown for the sake of clarity). The coordination of the carbohydrate in the binding sites is very well conserved for different GlcNAc ligands (mono-, di- and tetravalent). D) shows the result of a superposition of MUeSLI^{GlcNAc} onto the slightly different orientations of the carbohydrate in binding sites B_1C_2 and C_2B_1. E) Analysis of the deviations in the position of the nitroxide radical electron was performed by distance evaluation with the UCSF Chimera software: Assuming that the radical electron is delocalized over the entire N-O-bond length we measured distances between the O-atom used for prediction of the distances in Table 1 and the O- and N-atoms of the nitroxides of all other MUeSLI^{GlcNAc} conformations in the same binding site as indicated in E). The largest possible deviations between two positions of the electron of MUeSLI^{GlcNAc} located in the same binding site were found to be 2.2 Å for B_1C_2 (and 1.7 Å for C_2B_1). We therefore estimate the average deviation of the electron position at 1.1. Å per binding site and the average uncertainty in the distances at 2.2 Å.

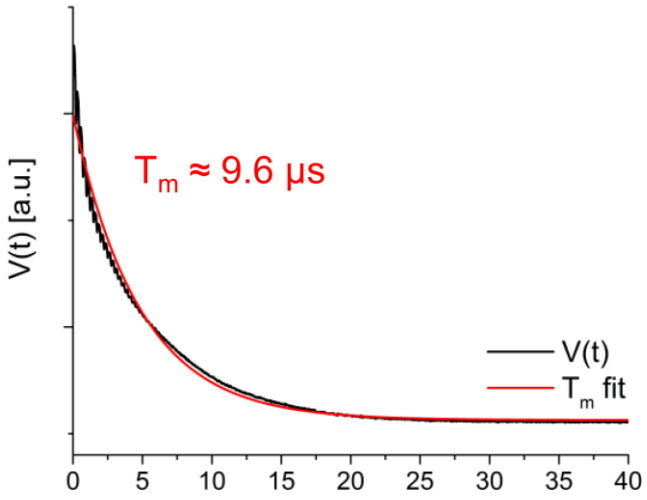

Figure S6: Phase memory time T_m of MUeSLI^{GlcNAc} DEER samples. T_m was determined at T = 50 K for a DEER sample containing 400 µM MUeSLI^{GlcNAc} in 2-fold molar excess over WGA dimer (200 µM). The figure shows experimental raw data (black line) and the fit performed with the exponential decay model $V(t) = V_0(t) \cdot \exp\left(-\frac{2t}{T_m}\right) + offset$ (red line). The best description of the experimental data is achieved with a phase memory time T_m = 9.6 µs. However, the first part of the T_m curve decays super-exponentially, most probably causing a slightly reduced T_m in the actual DEER measurement.

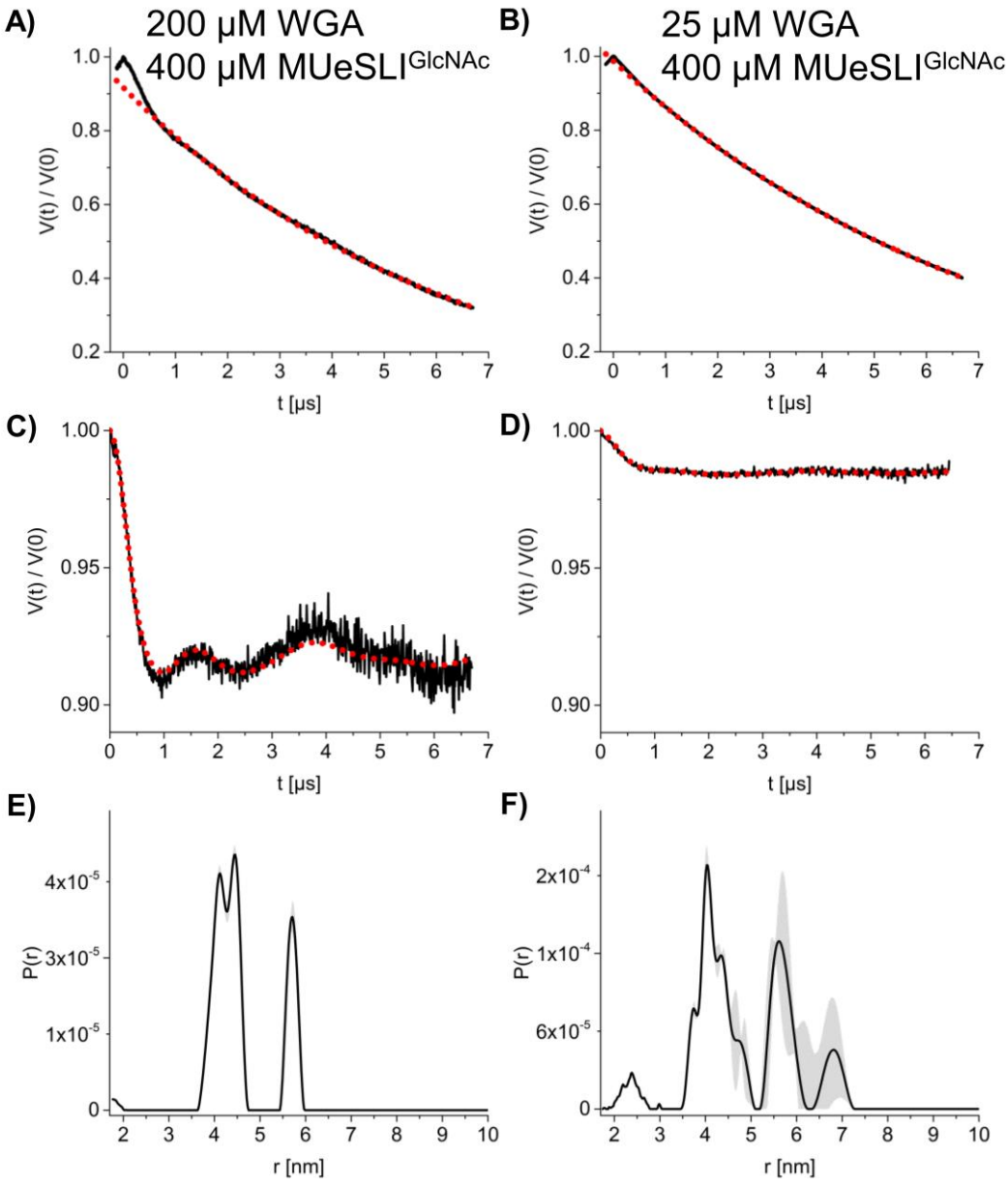

Figure S7: Q-band DEER of MUeSLI^{GlcNAc} with WGA. Q-band DEER experiments with MUeSLI^{GlcNAc} (400 µM) in 2-fold and 16-fold molar excess over WGA dimer (200 and 25 µM, respectively) were performed at T = 50 K. A) and B) show experimental raw data (black lines) and the 3-dimensional homogeneous background functions (red dotted lines). C) and D) show the form factor after background extraction (black lines) and the corresponding Tikhonov regularization fits (red dotted lines). Modulation depths are 8.3 and 1.3 %, respectively. (The fitting quality is not perfect in C) – see Figure S9 for further analysis.) E) and F) show the distance distributions obtained by Tikhonov regularization (black) with α parameters 28.5 and 24.1, respectively, as suggested by the L-curve criterion including the results of the validation (gray shaded area) obtained by DEERAnalysis 2016.

Experimentally, we find modulation depths $\Delta_{25\,\mu M}$ = 1.3 % and $\Delta_{200\,\mu M}$ = 8.3 % for DEER samples containing 25 µM WGA and 200 µM WGA, respectively. Intuitively, one might think that in the case of 16-fold molar excess of ligand the modulation depth should increase compared to a 2-fold molar excess.

However, both samples contain the same concentration of MUeSLI^{GlcNAc}, which is well below the dissociation constant K_d (compare Figure S1), while the protein amount is varied between the DEER samples in order to adjust the ratio of ligand vs. protein. Thus, while adjusting the ligand excess from 2-fold to 16-fold, the protein amount in the sample is reduced from 200 μM WGA to 25 μM WGA. In accordance with the equilibrium equation of the K_d value, the equilibrium is thereby further shifted away from the ligand-bound state. Hence, at 16-fold molar excess of ligand, less ligand is bound onto the protein, while most ligand molecules remain unbound in solution. This leads to a large background signal resulting from unbound ligand (or WGA occupied by only 1 ligand molecule) and to a very small modulation depth, which is even reduced in comparison to the sample with 2-fold molar excess of ligand.

The modulation depth Δ of a DEER experiment can be used to calculate the average number of spins *n* per nanoobject as $n = \frac{\ln(1-\Delta)}{\ln(1-\lambda)}$, where λ is the inversion efficiency for the specific experimental setup.[15] With an inversion efficiency of ≈ 22 % at our spectrometer and the experimental modulation depths $\Delta_{25\ \mu M}$ and $\Delta_{200\ \mu M}$, the corresponding average numbers of spin per nanoobject are $n_{25\ \mu M}$ = 1.05 and $n_{200\ \mu M}$ = 1.35. This is in accordance with the very low binding affinity of MUeSLI^{GlcNAc} to WGA. Assuming, that multi-spin situations with more than two MUeSLI^{GlcNAc} bound per WGA dimer are negligible given the low binding affinity and modulation depths, the fraction of spin-labeled MUeSLI^{GlcNAc} involved in complexes with WGA and two bound MUeSLI^{GlcNAc} can be determined as $x_d = \frac{\Delta}{\lambda}$ according to Ackermann et al.[16] For our DEER samples this gives a fraction of 5.9 % and 37.5 % of the total spin label concentration that is present in a doubly occupied protein complex for samples containing 25 μM WGA and 200 μM WGA, respectively.

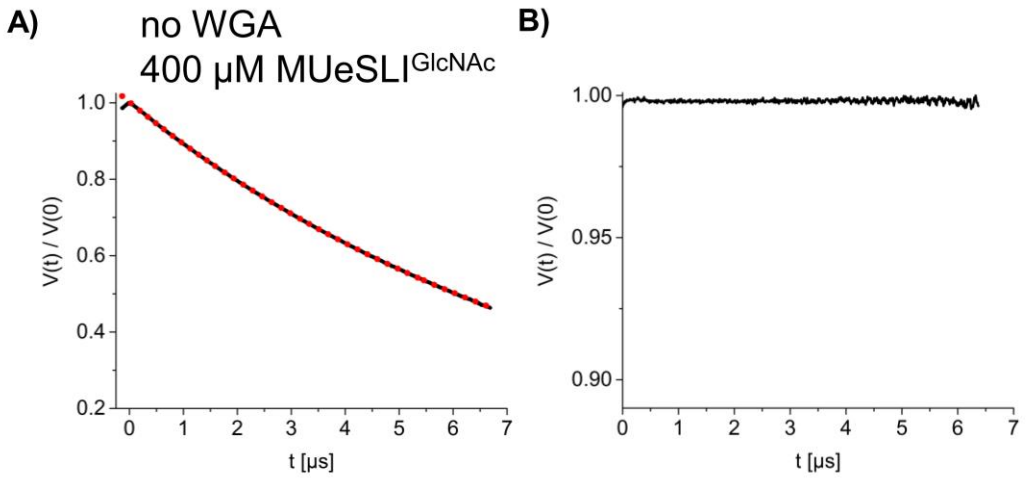

Figure S8: Q-band DEER of MUeSLI^{GlcNAc} in the absence of WGA. Q-band DEER experiments with MUeSLI^{GlcNAc} (400 µM) without WGA dimer were performed at T = 50 K. A) shows experimental raw data (black line) and the 3-dimensional homogeneous background function (red dotted line), which already describes the data set perfectly. B) shows the form factor after background extraction (black line). The modulation depth is 0 %, indicating that no residual dipolar couplings between the monovalent ligands are present. Therefore, this data set does not contain any distance information.

This result is a valuable control indicating that the very low modulation depth of 1.3 % observed for MUeSLI^{GlcNAc} in the presence of 25 µM WGA (see Figure S7) is not caused by residual dipolar couplings of monovalent MUeSLI^{GlcNAc}, but originates from ligands bound to WGA dimers and thus allows evaluation of the distance distribution.

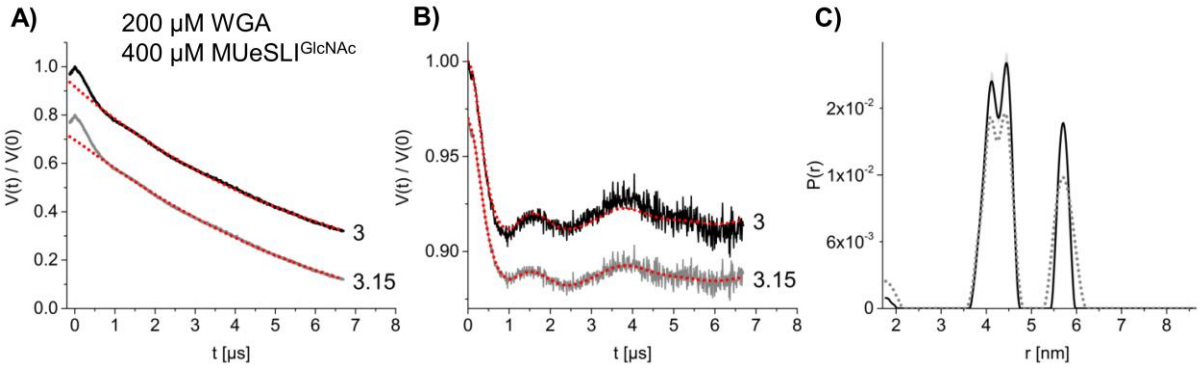

Figure S9: Analysis of DEER background function. As indicated in Figure S7 C), the Tikhonov fitting quality for the DEER sample containing 400 µM MUeSLI^{GlcNAc} and 200 µM WGA is suboptimal. While a reduced dipolar evolution time can help to improve the signal-to-noise ratio as well as the quality of the fit (data not shown), it prevents the reliable analysis of the longer distances in the distance distribution. Thus, a dipolar evolution time of 7 µs is the better choice in this case.

The suboptimal fitting quality of the Tikhonov regularization is due to imperfect background correction with a 3-dimensional homogeneous background function. Therefore, the influence of the background-dimension on the distance evaluation was analyzed by fitting the dimension of the background function. Best results were obtained for a background dimension of 3.15. A) shows the DEER raw data (black and gray) fitted with a 3- and 3.15-dimensional homogeneous background function (red dotted), respectively. B) shows the form factor after background correction with a 3- or 3.15-dimensional background function (black and gray, respectively) and the corresponding fit of the Tikhonov regularization. Notably, the signal-to-noise ratio as well as the fitting quality are increased for a 3.15-dimensional background function. C) shows the distance distribution obtained with the 3.15-dimensional background correction (gray dotted) in comparison to the distribution for a 3-dimensional background (black solid). The distance distribution remains unchanged while adjusting the background function. Thus, in order to be consistent with the other DEER data, a 3-dimensional background correction was used for data analysis.

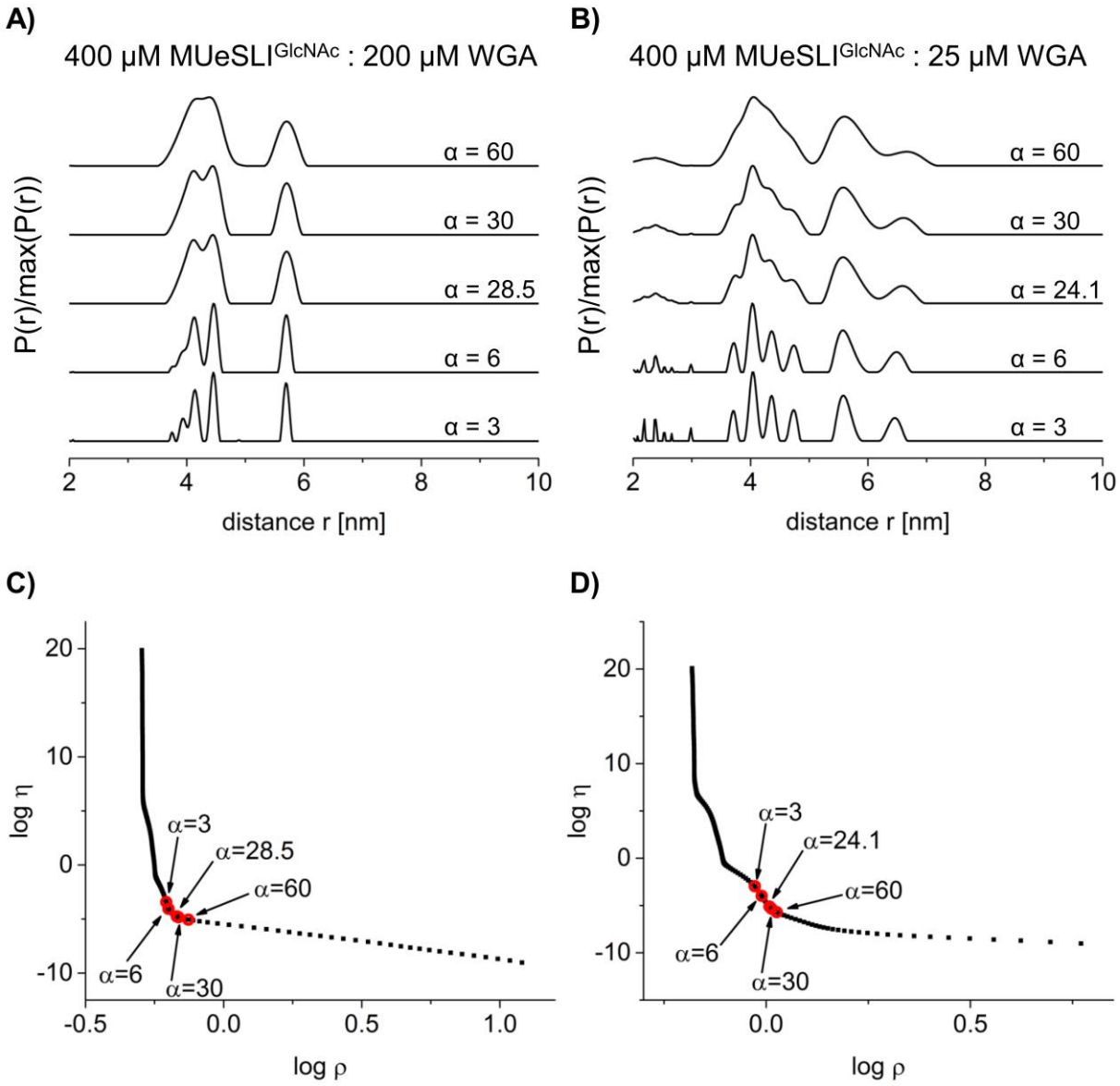

Figure S10: Consideration of the alpha parameters. The regularization parameter α for each distance distribution shown in Figure S5 was chosen according to the L-curve criterion. However, it was recently shown that the L-curve criterion has a tendency to oversmooth the data, which might also apply for MUeSLI with its well-defined spatial position of the radical electron.[17] Thus, we investigated the distance distributions obtained for various regularization parameters, finding that for a range of αs the observed peak patterns persist: (A) and (B) shown distance distributions (each normalized to the highest peak) obtained by Tikhonov regularization with different regularization parameters as indicated in (C) and (D). The regularization parameter influences the widths of the contributions to the distance distribution. However, the data analysis delivers very robust results for the range of α parameters applied for the data obtained with a ligand to protein ratio of 2:1 (A), as well as 16:1 (B).

For example, reducing the α parameter to α = 3, the width of the peaks at 5.6 nm becomes smaller. However, contributions expected for occupied sites A_1 and A_2 expected around 5.2 nm are still clearly missing from the distance distributions. Thus, we conclude that A_1 and A_2 binding sites are not occupied in solution in accordance with previous findings.[12]

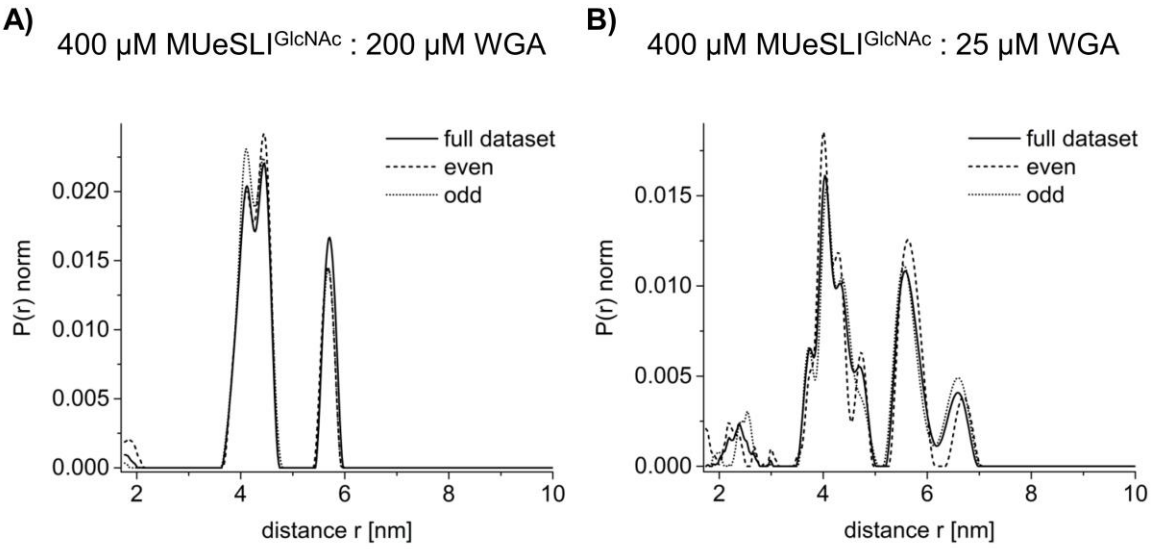

Figure S11: Persistence of peaks in the analysis of subsets of 2D DEER data. The two-dimensional data sets recorded for 400 µM MUeSLI^{GlcNAc} in the presence of 200 and 25 µM WGA dimer, respectively were each split into two subsets containing either only the even or only the odd scans of the DEER time trace. Independent data analysis of these subsets was performed as described in the experimental section and the results are displayed. The depicted probability distributions are normalized such that $\int P(r) = 1$. Only slight deviations are observed between the results of even, odd and full data sets. The persistence of the peaks in the distance distributions (also at the elevated noise level that comes with cutting the data in half) is a good indication for their reliability.

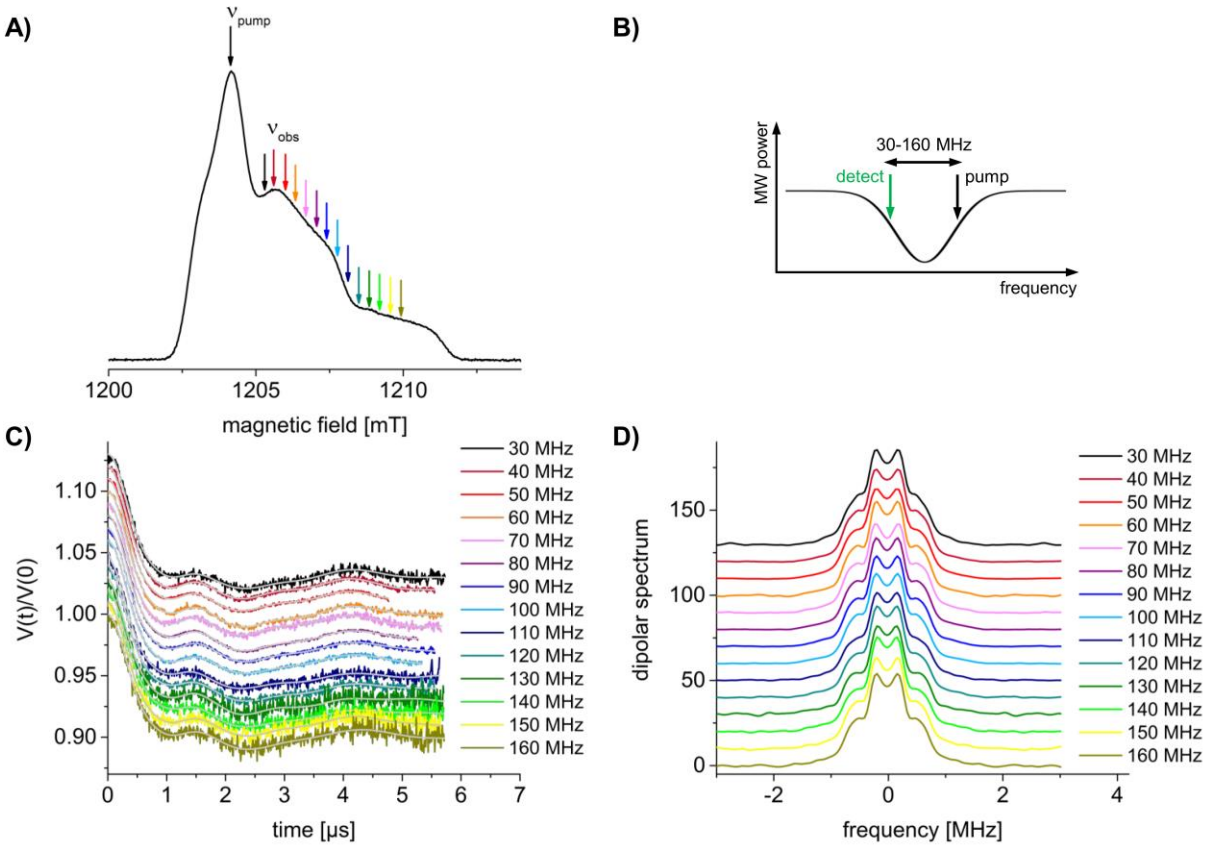

Figure S12: Orientation selection experiment. With a sample containing 200 µM WGA and 400 µM MUeSLI^{GlcNAc} orientation selection experiments were performed. A) The frequency separation between pump and observer pulses was varied between 30 and 160 MHz in steps of 10 MHz. B) The pump pulse was positioned on the maximum of the EPR spectrum, which was positioned 80 MHz above the resonator dip in order to account for limited resonator bandwidth. C) DEER time traces for all frequency offsets after background correction. For better visibility, traces were normalized to identical modulation depths of 10 % and shifted on the intensity axis. No dependence on the offset frequency can be determined in the time traces. D) Dipolar spectra corresponding to the DEER time traces for all offset frequencies. No significant changes depending on the offset frequency can be determined in the spectra.

Table S2

Table S2: EPR parameters of MUeSLI^{GlcNAc}. Parameters obtained by EPR spectral simulations for MUeSLI^{GlcNAc} from measurements performed in frozen solution at X-band and W-band frequencies. The g-tensor principal components were determined from the cw EPR spectrum recorded at W-band frequency at T = 175 K (Figure S2) and subsequently used for the simulation of the cw EPR X-band spectrum recorded at T = 120 K (Figure S1), where the g-tensor is not resolved. All given parameters are the mean values from a set of several full spectral simulations with different starting values, the corresponding standard deviations are given as error estimates in parentheses. The values obtained for the g-tensor components are in perfect agreement with values reported for TEMPONE.[18]

	A_{xx}/A_{yy} [MHz]	A_{zz} [MHz]	g_{xx}	g_{yy}	g_{zz}	lw[mT]
W-band	16.95 (±0.12)	95.99 (±0.092)	2.0094 (±0.0001)	2.0061 (±0.0001)	2.0021 (±0.0001)	0.84 (±0.036)
X-band	15.91 (±0.0043)	95.8 (±0.016)	2.0094 (±0.0001)	2.0061 (±0.0001)	2.0021 (±0.0001)	0.9 (±0.0022)

NMR Spectra

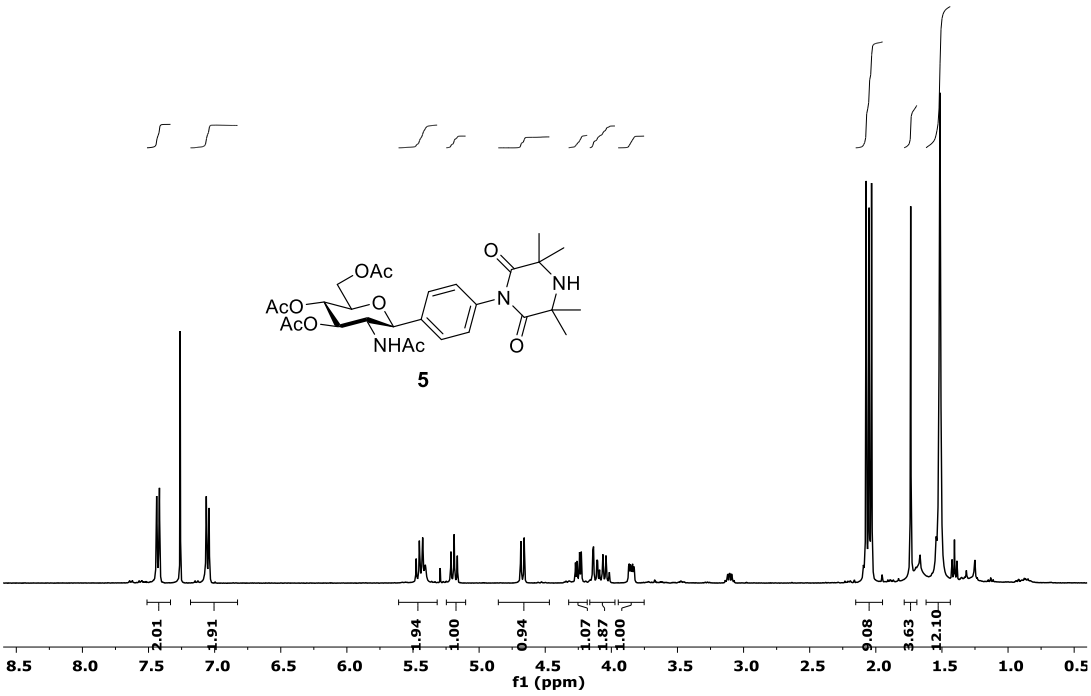

^{1}H NMR spectrum (400 MHz, $CDCl_3$) of **5**.

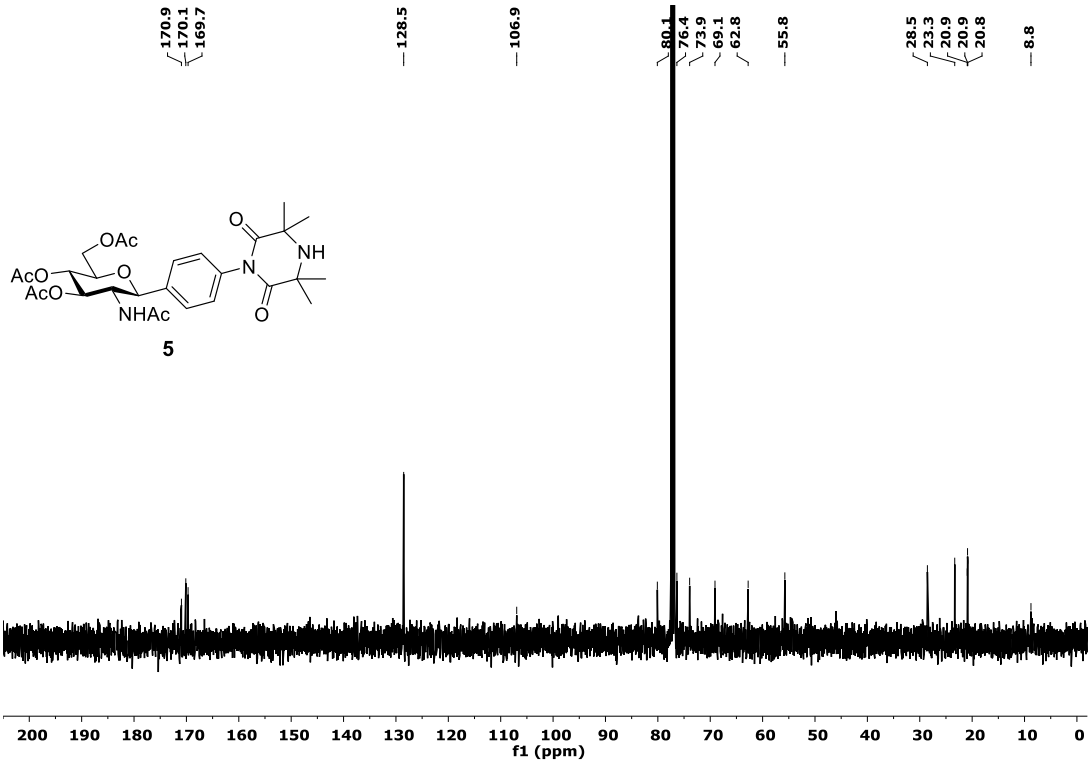

^{13}C NMR spectrum (100 MHz, $CDCl_3$) of **5**.

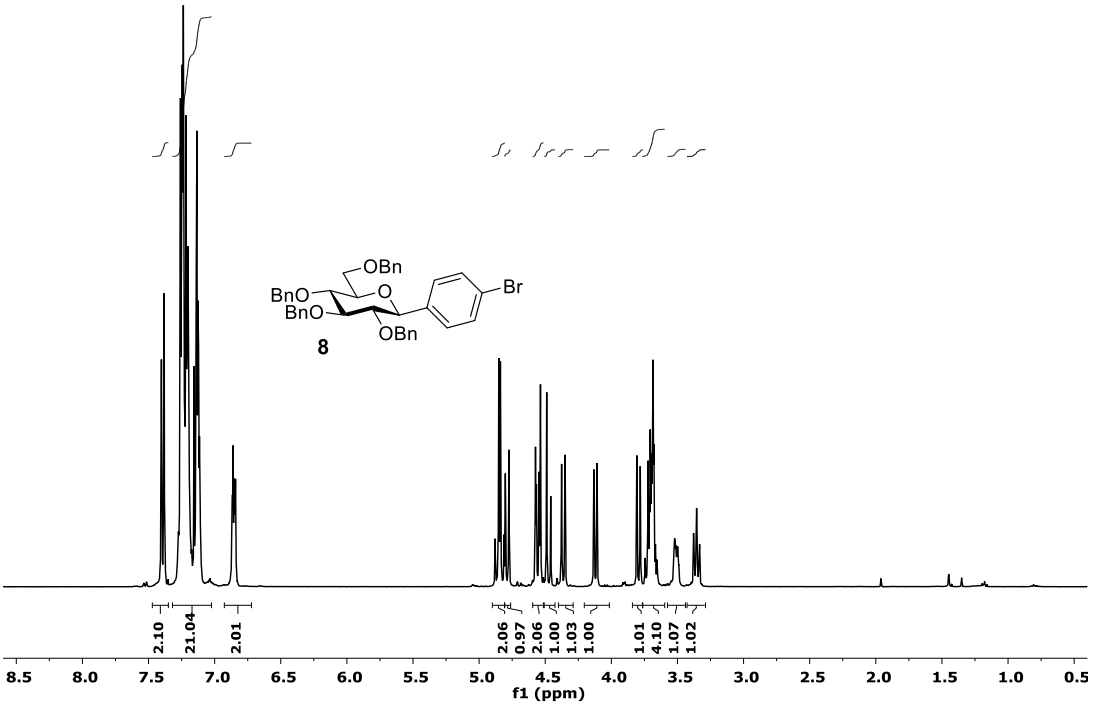

^{1}H NMR spectrum (400 MHz, $CDCl_3$) of **8**.

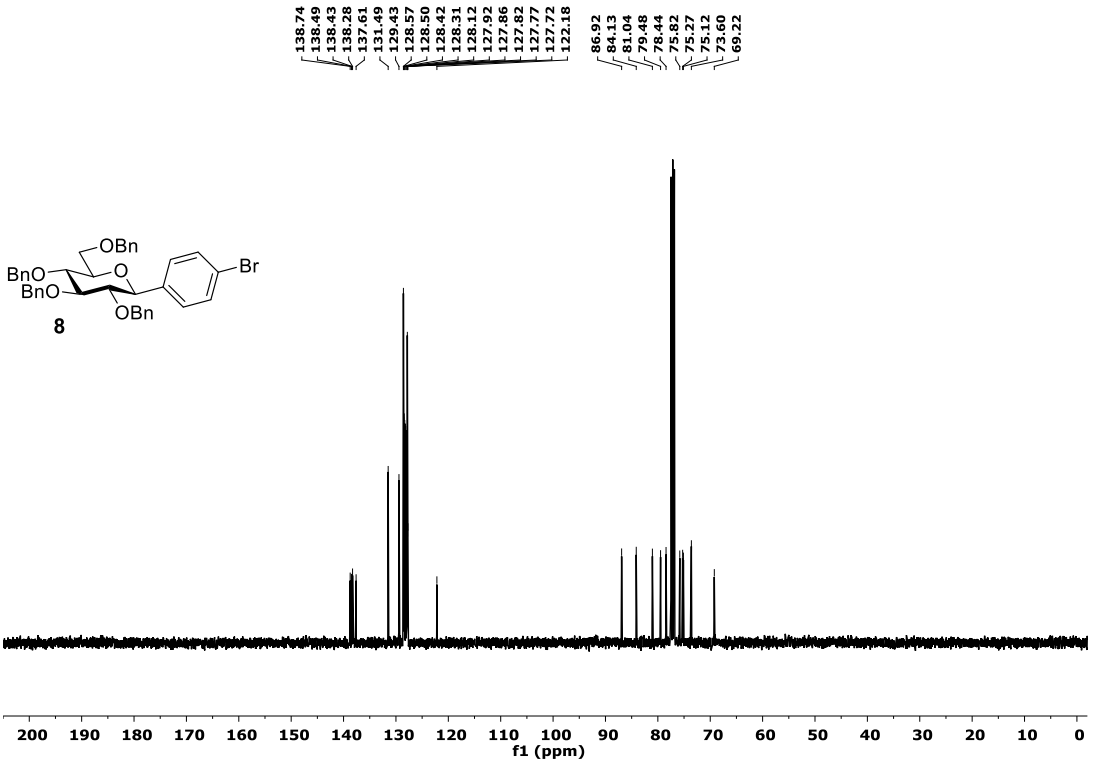

^{13}C NMR spectrum (100 MHz, $CDCl_3$) of **8**.

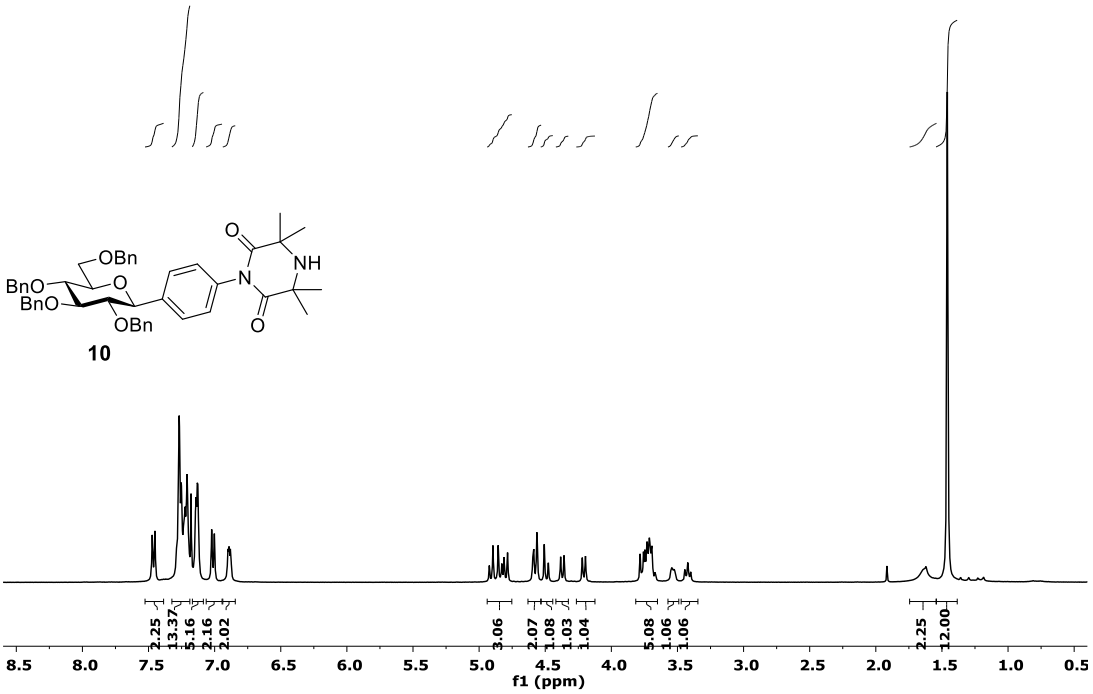

^{1}H NMR spectrum (400 MHz, $CDCl_3$) of **10**.

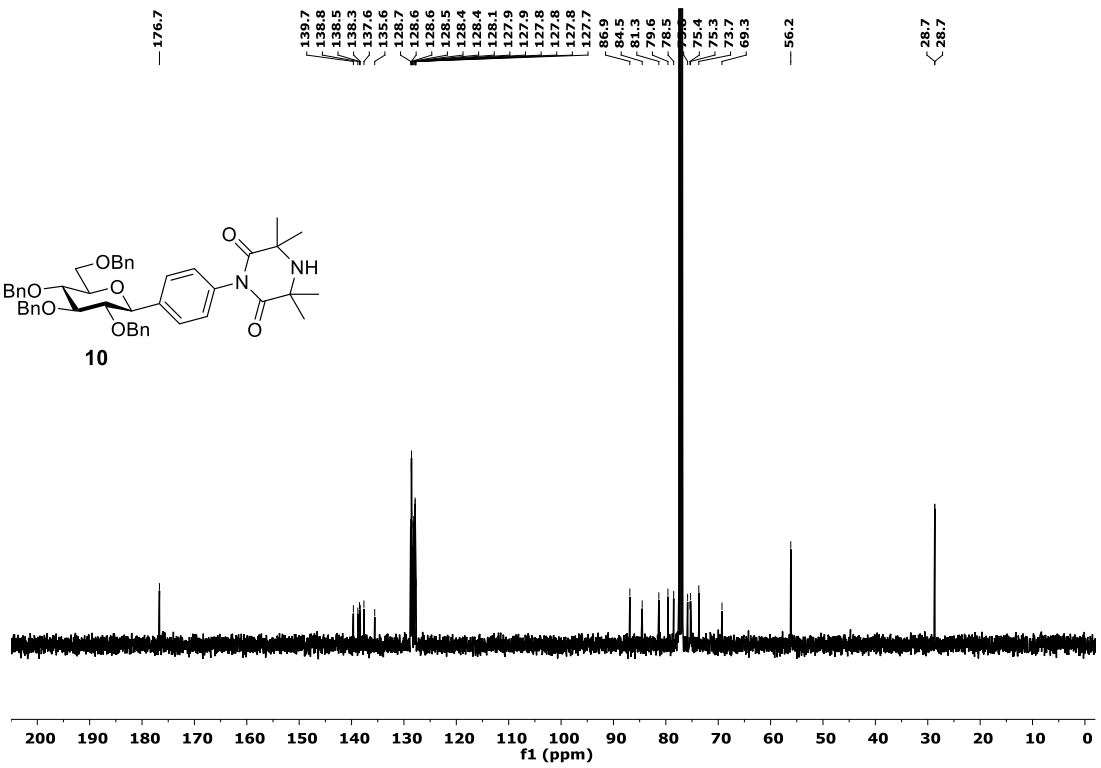

^{13}C NMR spectrum (100 MHz, $CDCl_3$) of **10**.

HPLC profiles of paramagnetic compounds

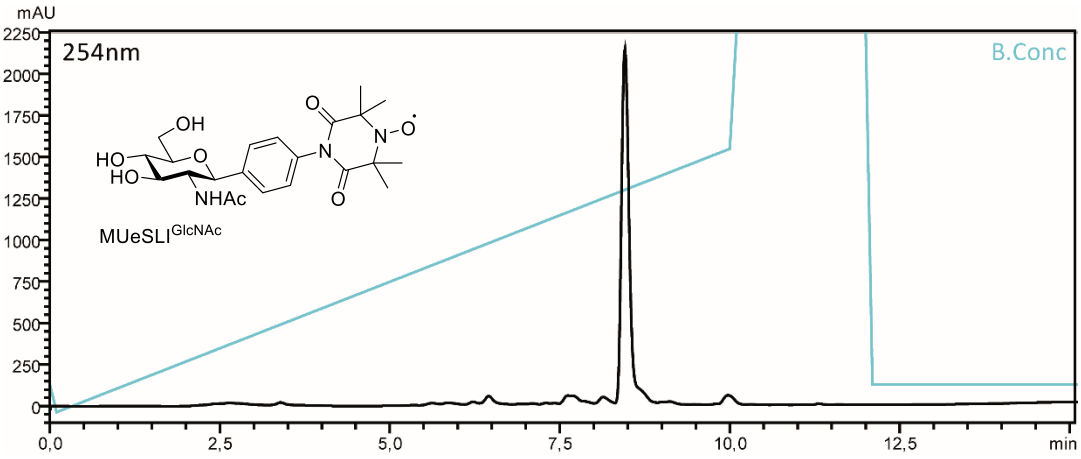

HPLC profile of MUeSLI^{GlcNAc} at 254 nm (Method: 3-70 % MeCN in 10 min).

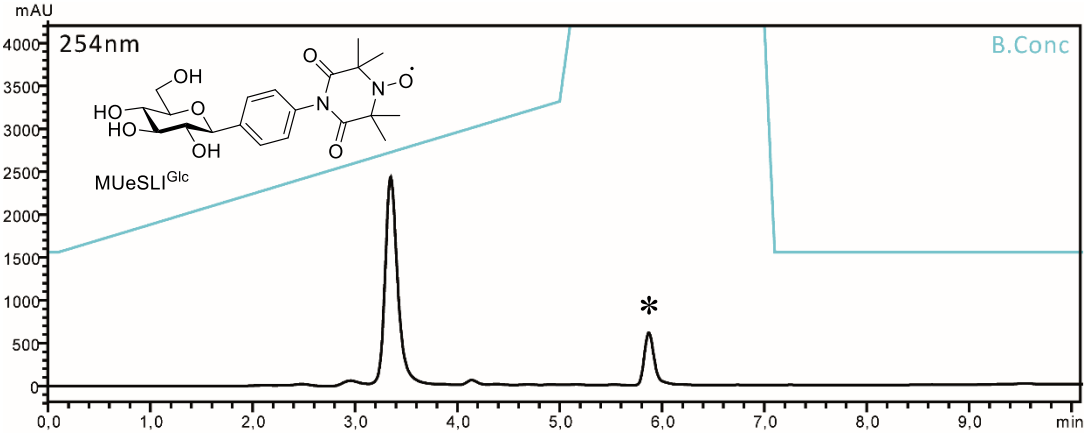

HPLC profile of MUeSLI^{Glc} at 254 nm (Method: 40-80 % MeCN in 5 min). * Non-product related peak resulting from column cleaning with 100 % MeCN.

References

[1] T. Seitz, C. Fleck, V. Wittmann, in *Carbohydrate Chemistry: Proven Synthetic Methods, Vol. 3* (Eds.: R. Roy, S. Vidal), CRC Press, Boca Raton, **2015**, pp. 219-225.

[2] S. Stoller, G. Sicoli, T. Y. Baranova, M. Bennati, U. Diederichsen, *Angew. Chem., Int. Ed.* **2011**, *50*, 9743-9746.

[3] S. Stoller, G. Sicoli, T. Y. Baranova, M. Bennati, U. Diederichsen, *Angew. Chem.* **2011**, *123*, 9917-9920.

[4] R. Benhaddou, S. Czernecki, W. Farid, G. Ville, J. Xie, A. Zegar, *Carbohydr. Res.* **1994**, *260*, 243-250.

[5] S. Stoll, A. Schweiger, *J. Magn. Reson.* **2006**, *178*, 42-55.

[6] J. Krzystek, A. Sienkiewicz, L. Pardi, L. C. Brunel, *J. Magn. Reson.* **1997**, *125*, 207-211.

[7] J. Weil, J. Bolton, J. Wertz, in *Elementary Theory and Practical Applications*, Wiley and Sons New York, **1994**.

[8] M. Pannier, S. Veit, A. Godt, G. Jeschke, H. W. Spiess, *J. Magn. Reson.* **2000**, *213*, 316-325.

[9] G. Jeschke, V. Chechik, P. Ionita, A. Godt, H. Zimmermann, J. Banham, C. R. Timmel, D. Hilger, H. Jung, *Appl. Magn. Reson.* **2006**, *30*, 473-498.

[10] G. Bains, R. T. Lee, Y. C. Lee, E. Freire, *Biochemistry* **1992**, *31*, 12624-12628.

[11] A. Kristiansen, Å. Nysæter, H. Grasdalen, K. M. Vårum, *Carbohydr. Polym.* **1999**, *38*, 23-32.

[12] D. Schwefel, C. Maierhofer, J. G. Beck, S. Seeberger, K. Diederichs, H. M. Moller, W. Welte, V. Wittmann, *J. Am. Chem. Soc.* **2010**, *132*, 8704-8719.

[13] E. F. Pettersen, T. D. Goddard, C. C. Huang, G. S. Couch, D. M. Greenblatt, E. C. Meng, T. E. Ferrin, *J. Comput. Chem.* **2004**, *25*, 1605-1612.

[14] C. S. Wright, *J. Mol. Biol.* **1990**, *215*, 635-651.

[15] B. E. Bode, D. Margraf, J. Plackmeyer, G. Dürner, T. F. Prisner, O. Schiemann, *J. Am. Chem. Soc.* **2007**, *129*, 6736-6745.

[16] K. Ackermann, A. Giannoulis, D. B. Cordes, A. M. Slawin, B. E. Bode, *Chem Commun (Camb)* **2015**, *51*, 5257-5260.

[17] T. H. Edwards, S. Stoll, *J. Magn. Reson.* **2018**, *288*, 58-68.

[18] W. Snipes, J. Cupp, G. Cohn, A. Keith, *Biophys. J.* **1974**, *14*, 20-32.